Development of Si–SiC Hybrid Structures for Elevated Temperature Micro-Turbomachinery

Hyung-Soo Moon, Dongwon Choi, and S. Mark Spearing, *Member, ASME*

***Abstract*—The design of the Massachusetts Institute of Technology (MIT) microengine is limited in part by the material capability of Si primarily due to the pronounced thermal-softening and strain-softening at temperatures higher than the brittle-to-ductile transition temperature (BDT), approximately 550 °C. In order to circumvent this limitation, it has been proposed to reinforce the Si with chemical vapor deposited (CVD) SiC in strategic locations to create a Si–SiC hybrid microengine turbine spool. Detailed design of Si–SiC hybrid structures for high temperature micro-turbomachinery, however, has been hampered by the lack of understanding of the mechanical behavior of Si and SiC hybrid structures at elevated temperatures and by the unavailability of accurate material properties data for both Si and SiC at the temperatures of interest. In this work, a series of initial thermomechanical FE analyzes have been performed to assess the advantage of the hybrid structures, and to provide structural design criteria and fabrication requirements. Then, the feasibility of the Si–SiC hybrid structures concept for elevated temperature micro-turbomachinery was verified based on more rigorous mechanical testing at high temperatures. Finally, the Si–SiC hybrid spool design was critically reevaluated with regard to creep using a Si constitutive model developed as a separate effort. [0988]**

***Index Terms*—Finite element analysis, mechanical testing, Massachusetts Institute of Technology (MIT) microengine, Si–SiC hybrid structures.**

I. Introduction

SINGLE crystal silicon, the material of choice for the first MIT (demonstration) microengine [1], exhibits strong thermal-softening behavior at temperatures higher than its brittle-to-ductile transition temperature (BDT), approximately 550 °C. This thermal softening behavior limits the turbine inlet temperature, which in turn significantly degrades the overall engine efficiency. Thus, the strategy employed in the all-silicon demonstration engine [2], [3] was to design the rotor so that there is a high heat flux from the turbine rotor to the compressor to keep the wall temperature of the turbine rotor below 650 °C, at which temperature the Si yield strength is on the order of 250 MPa. This strategy, while permitting a workable demonstration device, has a severe negative impact on the engine efficiency and power output.

Manuscript received January 13, 2003; revised August 15, 2003. This work was supported by ARO MURI under Contract DAAG55-98-1-0292. Subject Editor C.-J. Kim.

H.-S. Moon and S. M. Spearing are with the Department of Aeronautics and Astronautics Engineering, Massachusetts Institute of Technology, Cambridge, MA 02139 USA (e-mail: hsmoon@mit.edu; spearing@mit.edu).

D. Choi is with the Department of Material Science and Engineering, Massachusetts Institute of Technology, Cambridge, MA 02139 USA (e-mail: dwchoi@mit.edu).

Digital Object Identifier 10.1109/JMEMS.2004.832182

In order to improve the microengine's performance, the heat flux from the turbine into the compressor must be reduced by introducing a thermal barrier structure between the turbine and compressor. Decreasing the heat flux, however, implies that the turbine wall temperature may increase higher than silicon can withstand. In order to circumvent this limitation, it has been proposed to reinforce the Si with chemical vapor deposition (CVD) SiC in strategic locations to create Si–SiC hybrid structures for elevated temperature micro-turbomachinery [4], [5]. The proposed conceptual design of a Si–SiC hybrid rotor structure is shown schematically in Fig. 1. The rationale that led to this structural design has been discussed in more detail together with preliminary structural analyzes and its contributions to the overall engine performance in [6]. While this previous work has assessed the potential of the Si–SiC hybrid structures for improving engine efficiency as well as maintaining structural integrity, it has not accounted for the effects of the pronounced strain-softening and creep of Si at elevated temperatures and high stresses. Furthermore, the stress concentration within a part made of single crystal Si exhibiting the strain-softening behavior may accelerate and propagate the localized deformation, as pointed out by Walters [7], [8].

This paper focuses on developing a self-consistent design for Si–SiC hybrid structures for elevated temperature micro-turbomachinery, powerMEMS, given the constraints imposed by microfabrication processes and system considerations. In Section II, a brief description of the status of the Si–SiC microfabrication process is presented. Section III presents a series of initial thermomechanical FE analysis results for Si–SiC hybrid structures to assess the feasibility of the hybrid structures, and to provide structural design criteria and fabrication requirements. Materials and structures issues associated with the mechanical characteristics of Si at elevated temperatures in the development of Si–SiC hybrid structures for micro-turbomachinery are also addressed. In Section IV, the feasibility of the Si–SiC hybrid structures concept for elevated temperature micro-turbomachinery is verified based on rigorous mechanical testing at high temperatures. Finally, the Si–SiC hybrid spool design is critically re-evaluated with regard to creep using an Si constitutive model developed as a separate effort.

II. Si–SiC Microfabrication Process

SiC has been identified as the most promising candidate for use as a refractory structural material due to its high stiffness, strength, and chemical stability at elevated temperatures [9], [10]. However, techniques for microfabricating single crystalline SiC to the high level of precision required for the microengine are not yet available primarily due to the lack of

1057-7157/04$20.00 © 2004 IEEE

Authorized licensed use limited to: UNIVERSITY OF SOUTHAMPTON. Downloaded on July 1, 2009 at 12:12 from IEEE Xplore. Restrictions apply.

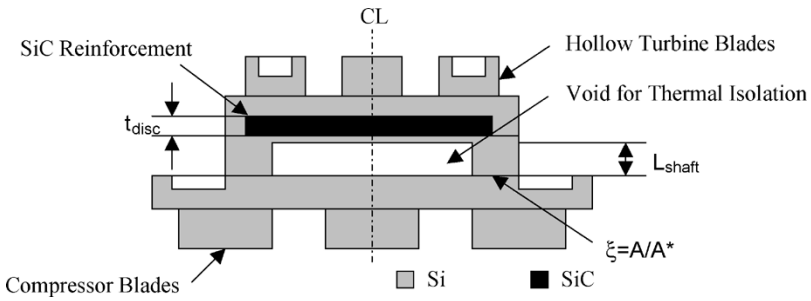

Fig. 1. Cross section of the proposed conceptual design of a Si–SiC hybrid rotor. Critical dimensions and parameters are shown.

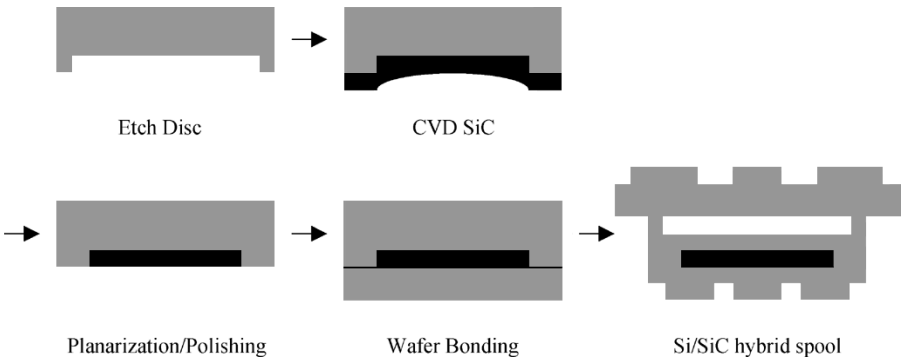

Fig. 2. Si–SiC hybrid spool process steps.

precise and fast SiC etching techniques. To circumvent this limitation, CVD of polycrystalline SiC coatings on silicon wafers has been utilized to fabricate the Si–SiC hybrid structures. The necessary process steps required for the Si–SiC hybrid turbine structures are outlined in Fig. 2. CVD SiC is deposited on pre-patterned silicon wafers and the wafers with thick SiC coatings are then fabricated into turbine rotors by post-CVD processes such as wafer planarization, wafer bonding, and deep-reactive ion etching (DRIE).

A. LPCVD SiC and Residual Stress Control

CVD SiC is deposited on 100 mm, n-type, (100) silicon wafers by the thermal decomposition of vaporized methyltrichlorosilane (MTS) using hydrogen as a carrier gas at elevated temperatures and subatmospheric pressures according to the following chemical reaction [5], [11], [12]:

$$\mathrm{CH_3SiCl_3} + \alpha\mathrm{H_2} \rightarrow \mathrm{SiC} + 3\mathrm{HCl} + \alpha\mathrm{H_2}$$

where α is the molar ratio of $\mathrm{H_2}$ to $\mathrm{CH_3SiCl_3}$. The deposition temperature is around 1000 °C at which polycrystalline 3C-SiC with a zinc-blende structure is produced. SiC films produced at different temperatures and deposition rates have different grain sizes of approximately 50–200 nm. However, all the SiC films show columnar microstructures with a strong preferred orientation of (111) plane. Various systems and growth procedures for CVD SiC have been reported elsewhere [13]–[16]. Material characterization has shown that CVD SiC meets the major property requirements for the microengine such as high strength and conformality. The most critical issue in the SiC deposition is residual stress control. Controlling residual stresses by changing CVD process variables properly is of critical importance to all the Si–SiC hybrid structure fabrication steps since a high level of residual stress can cause wafer cracking during the deposition and planarization as well as excessive wafer bow, which is detrimental to the subsequent planarization and bonding processes. The stress development in the polycrystalline CVD SiC is associated with the presence of thermal and intrinsic stress components. Thermal stress develops in the SiC film during cooling to room temperature after deposition due to the thermal mismatch between the SiC and the Si substrate. Intrinsic stresses are associated with the microstructures determined by the material deposition and growth. One has more control of intrinsic stresses versus thermal stress simply because not much can be done about the thermal expansion coefficients of materials. Therefore, the basic concept of residual stress control is to balance the intrinsic stress components with the thermal stress component by modifying properly the CVD process parameters such as source gas ratio and deposition temperature. More details on the residual stress control in CVD SiC can be found in [11], [12], [17].

B. SiC Planarization and Wafer-Level Bonding Using Interlayer Material

Following SiC deposition, unnecessary parts of the SiC coatings are removed by planarization and polishing processes prior to bonding. For good wafer bonding, it is required to achieve a high degree of surface smoothness after planarization. In the case of Si-Si wafer bonding, it has been observed that the roughness of wafer surfaces should be less than about 10 Å [18]. The surface finishing of SiC is much more challenging because of its very high hardness and chemical stability. Due to the chemical inertness of SiC, Chemical Mechanical Polishing

Authorized licensed use limited to: UNIVERSITY OF SOUTHAMPTON. Downloaded on July 1, 2009 at 12:12 from IEEE Xplore. Restrictions apply.

(CMP) is not yet available to improve the surface smoothness of SiC to the level adequate for direct wafer bonding. Therefore, the current planarization technique adopted in this research uses only mechanical polishing with a diamond grit. However, use of a diamond grit unavoidably results in a rough hill-and-valley-like surface structure, which cannot meet the requirements for successful wafer-level bonding. To circumvent this problem, interlayer materials must be deposited on the rough surface of the polished SiC to fill the grooves introduced by the grinding/polishing processes. A CVD silicon oxide has been used as such an interlayer material, but oxide CMP is still necessary since the as-deposited surface of the CVD oxide is not smooth enough for direct wafer bonding either. Following the oxide CMP, H_2O_2-based standard RCA wet cleaning process is performed to remove any organic and metallic contaminants on all the surfaces to be bonded. The RCA cleaning also makes the wafer surfaces hydrophilic, which is required to facilitate spontaneous bonding upon wafer contact before finalizing the bonding process by high temperature annealing.

III. Si–SiC Hybrid Structures for Micro-Turbomachinery

As an extension of Miller's preliminary analysis [6], the structural analysis for the microengine focused on predicting the maximum operating temperature that the proposed hybrid structures could withstand and assessing the benefits from the spool design from the point of view of the overall engine efficiency. This section also addresses an assessment of the potential problems associated with the mechanical behavior of Si at elevated temperatures which have not previously been considered in detail.

A. Preliminary FE Analysis of Hybrid Turbine Rotor

Three-dimensional FE simulations for a hybrid turbine rotor have been performed with a refined FE model combining the turbine disc and blade as shown in Fig. 3 in order to verify the previous structural analysis by Miller [6], where the hybrid turbine blade and disc were considered as separate bodies. The FE mesh was created using a commercial pre-/post-processing package, MSC/PATRAN [19], and analyzed using ABAQUS STANDARD [20], a commercially available finite element package. A relative SiC thickness of 30%, the ratio of the SiC layer thickness against the Si–SiC hybrid disc thickness, was incorporated in the turbine rotor disc in between Si disc layers. This is consistent with the projected capabilities of the SiC deposition process. While SiC, whose melting point is 3000 °C, was assumed to behave elastically throughout the temperature range (up to 900 °C), the material model for Si was assumed to be elasto-plastic as modeled by ABAQUS STANDARD PLASTICITY with no strain-hardening/softening behavior. The thermal softening behavior of Si was described with the yield strength decreasing with increasing wall temperature according to

$$\sigma_Y = -A^*T + B \tag{1}$$

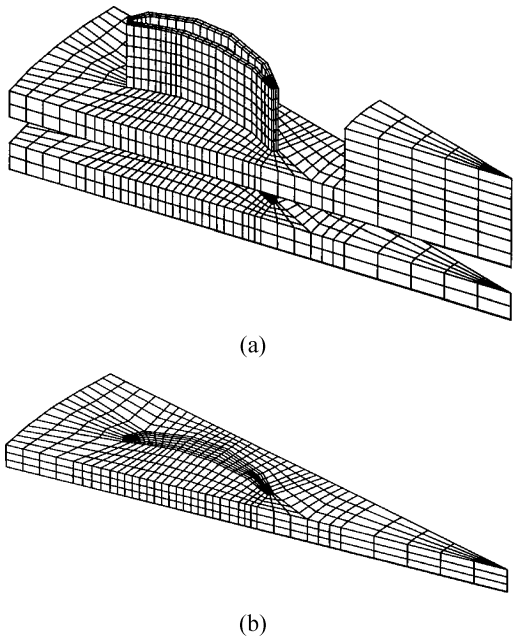

Fig. 3. Refined FE model for blade and disc (a) FE mesh for the Si and (b) FE mesh for the SiC.

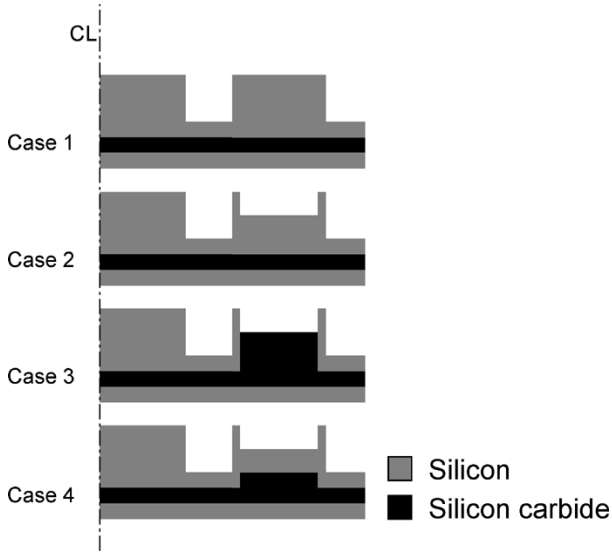

Fig. 4. Geometrical configurations considered in the analysis.

where A and B are the linear fit coefficients. Values of $A = 0.652\ \mathrm{MPa/K}$ and $B = 806.3\ \mathrm{MPa}(500 < T < 1220\ \mathrm{K})$ were used in the present analysis [6], [21]. Assuming that the periodic boundary condition has little influence on the overall deformation and stress fields of the rotor, only one twentieth of the turbine rotor was modeled. For simplicity, the thermal barrier (hollow shaft) was modeled as a linear spring.

As illustrated in Fig. 4, the geometrical configurations considered here were as follows:

1) solid silicon blade and disc reinforcement with 30% SiC;
2) all-silicon hollow blade with a half-height inner core and disc reinforcement with 30% SiC;
3) hybrid Si–SiC hollow blade with a half-height SiC inner core and disc reinforcement with 30% SiC;

Authorized licensed use limited to: UNIVERSITY OF SOUTHAMPTON. Downloaded on July 1, 2009 at 12:12 from IEEE Xplore. Restrictions apply.

TABLE I
SUMMARY OF FE CALCULATIONS OF THE Si–SiC HYBRID TURBINE ROTOR

Case	Max. Temp. [°C]	Max. stress in SiC [MPa]	Max. radial expansion [μm]	Max. tangential deflection [μm]	Max. vertical deflection [μm]
Solid Si blade + 30% SiC disc	890	514	2.2	1.8	4.6
All Si hollow blade + 30% SiC disc	905	509	2.1	2.0	4.0
Hollow Si blade w/ 50% SiC core + 30% SiC disc	920	644	2.4	1.6	5.8
All Si hollow blade w/ SiC post up to blade root + 30% SiC disc	905	510	2.0	1.7	3.9

*Stress and deflection values are obtained at the corresponding maximum temperature.

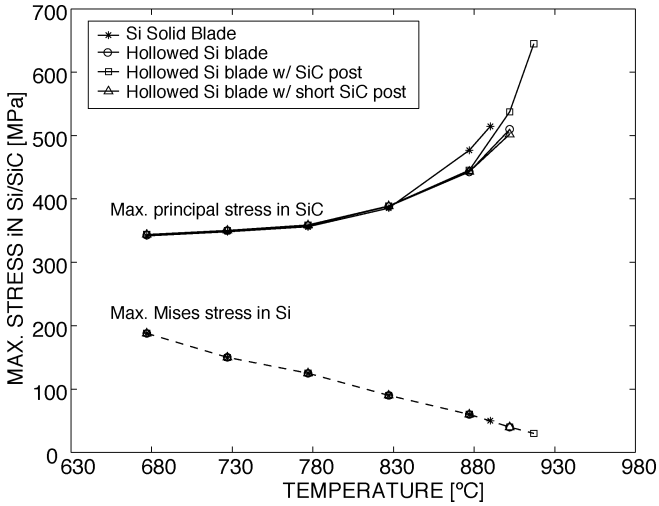

Fig. 5. Maximum stresses in the Si–SiC hybrid turbine rotor of four design configurations.

4) all-silicon hollow blade with a half-height inner core and SiC post up to blade roots and disc reinforcement with 30% SiC.

Fig. 5 shows how the maximum stresses for each case vary as the temperature increases. The results are summarized in Table I. This refined 3-D FE simulation correlates well with the previous hybrid disc and blade analysis by Miller [6] in terms of the prediction of the maximum turbine wall temperature that the hybrid structure can withstand. In conclusion, the FE simulation results confirm the potential of the hybrid structure concept for improving engine efficiency. Although there is little difference in the achievable maximum operating temperature among the four cases, Case 2 (all-silicon hollow blade and disc reinforced with SiC) stands out as a prospective candidate for the hybrid turbine rotor when microfabrication difficulties are taken into account.

B. Thermomechanical FE Analysis of Turbine Rotor

The structural analysis results in the previous section were obtained assuming uniform temperature in the turbine rotor, which is a reasonable assumption, given the low Biot number of approximately 0.02. The isothermal assumption, however, may not be valid when there is a heat sink (i.e., the compressor) that gives rise to a high thermal gradient. Thus, in order to identify any hot spots in the structure that may cause a catastrophic failure when combined with high local stresses, a 3-D thermomechanical FE analysis has been performed using the same FE mesh. It is critical that accurate thermal boundary conditions, which are not always readily available, be applied in the analysis. The thermal boundary conditions shown in Fig. 6 were based on the previous analysis [21] and the CFD results [22]. For simplicity, the thermal barrier structure (hollow shaft) is again modeled structurally as a linear spring.

As is clear in Fig. 7(a), the temperature distribution of the turbine rotor with a shaft/ring of 1.5 mm inner radius, 100 μm wall thickness, and 600 μm shaft length, shows a considerable temperature gradient. The highest temperature occurs at the tip of the blade and the lowest at the area adjacent to the shaft end. Fig. 7(b) and (c) show the effective stress and effective plastic strain, respectively, corresponding to the temperature field. While the high stress state of the SiC in the center indicates that the centrifugal inertial load is carried mostly by the SiC reinforcement, the high stress in the SiC reinforcement below the blade trailing edge is caused by the bending moment due to the blades. The plastic strain developed on the surface of the turbine rotor disk shown in Fig. 7(c) implies that the elastic material around the deformed zone is still sufficient to support the centrifugal loading.

C. Structural Analysis of Thermal Barrier

The small Biot number of the rotor implies that in order to improve the engine efficiency a significantly low thermal conductance ($1/R_{\rm th} = k_{\rm th}A^*/L$, where $k_{\rm th}$ is the thermal conductance of Si, A^* the area that contacts with the rotor, and L the length of the shaft) is required. This in turn may compromise the overall strength of the structure. In addition the difficulties associated with the deep etching process for the journal bearing face and wafer bonding process impose severe geometrical constraints on the achievable wall thickness and shaft length. For simplicity, the turbine blades and compressor blades were modified so as to apply the equivalent bending moment to

Authorized licensed use limited to: UNIVERSITY OF SOUTHAMPTON. Downloaded on July 1, 2009 at 12:12 from IEEE Xplore. Restrictions apply.

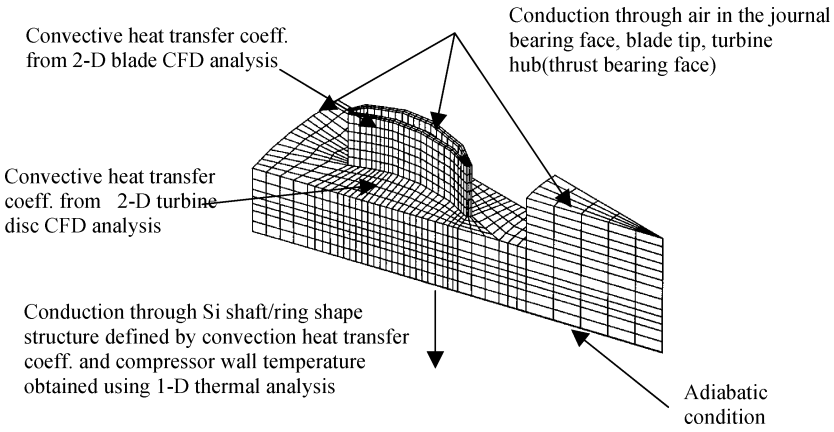

Fig. 6. Thermal boundary condition for the turbine rotor.

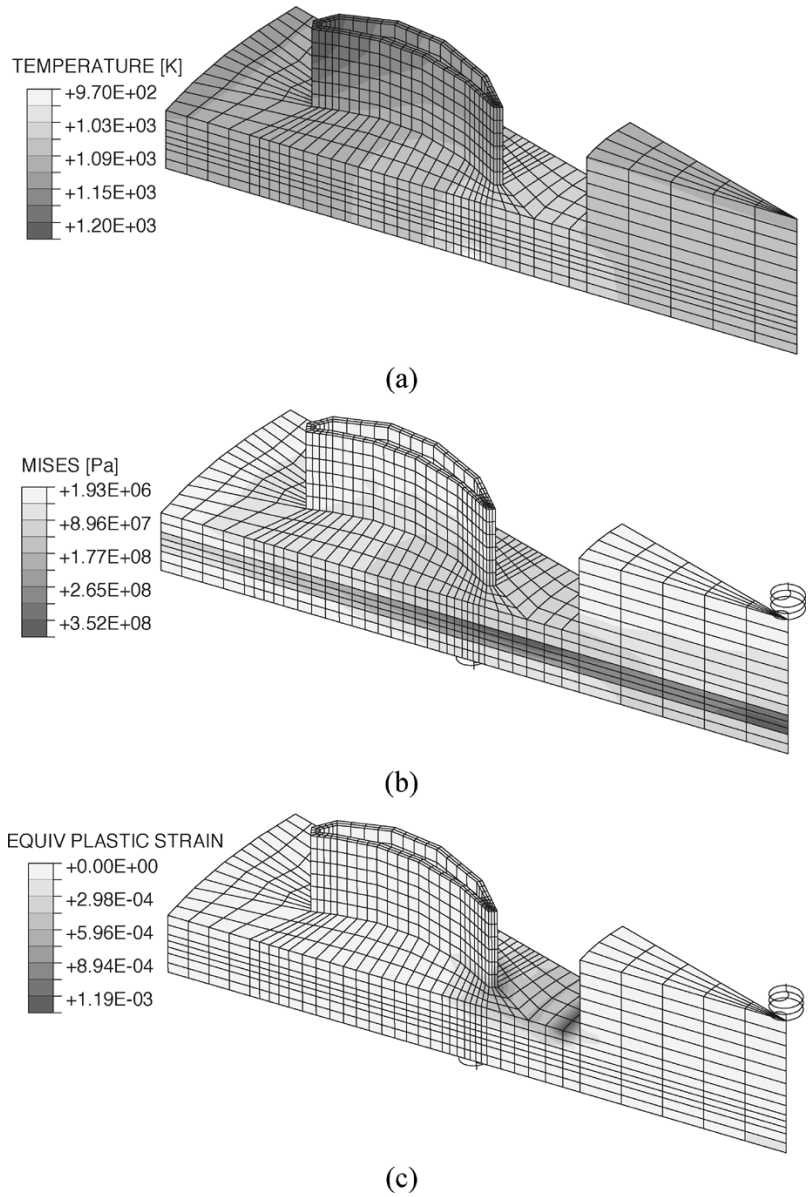

Fig. 7. Thermomechanical FE analysis results of a turbine rotor when $R_i = 1.5$ mm, $t_{\rm wall} = 100\ \mu$m, $L_{\rm shaft} = 600\ \mu$m}, (a) temperature distribution, (b) effective stress distribution, and (c) effective plastic strain.

the shaft so that an axisymmetric FE model can be used. The thermal boundary conditions were again based on the previous analysis [21]. Fig. 8 shows the FE results of the thermal insulation structure between the turbine and compressor rotors in the case where $A/A^* = 0.2$ ($R_i = 1.5$ mm, $t_{\rm wall} = 0.4\ \mu$m, and $L_{\rm shaft} = 0.4\ \mu$m). The temperatures at both ends of the

Authorized licensed use limited to: UNIVERSITY OF SOUTHAMPTON. Downloaded on July 1, 2009 at 12:12 from IEEE Xplore. Restrictions apply.

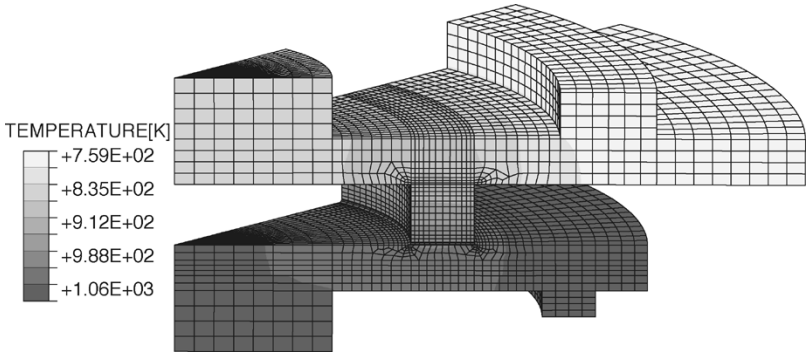

Fig. 8. FE mesh for the thermal insulation structure between the turbine and compressor disks in the case where $A/A^* = 0.2$ ($R_i = 1.5$ mm, $t_{\rm wall} = 0.4$ μm, and $L_{\rm shaft} = 0.4$ μm).

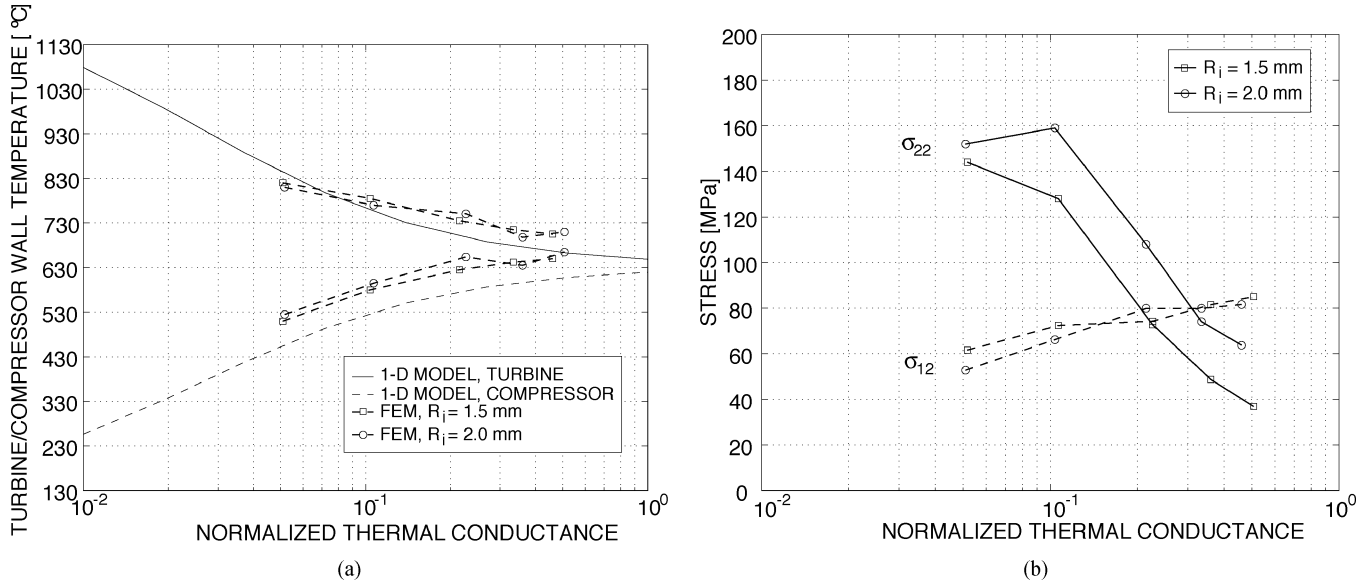

Fig. 9. Comparison for the FE results of thermal insulation structure with a 1-D cycle analysis, (a) temperatures of the both ends of the shaft and (b) stresses on the corner of the shaft.

shaft are plotted on Fig. 9(a) together with predictions using the 1-D thermal cycle analysis by Protz [3]. In Fig. 9(b), the stress states as a function of normalized thermal conductance are shown. Both the shear stress and normal stress were induced due to the bending moment from the blades and the discrepancies in the radial expansion of the turbine and compressor rotors. From the FE results, it is concluded that given the microfabrication limits, a thermal barrier structure is feasible, satisfying both thermal and structural requirements.

D. Materials and Structures Issues in the Design of Si–SiC Hybrid Structures

While the initial structural analysis presented so far verified the potential of Si–SiC hybrid structures as a medium term approach to improving the overall engine efficiency, the primary concerns associated with the mechanical behavior of Si at elevated temperatures remained unresolved. At the temperatures higher than the design temperature for the all-silicon microengine, the design of the turbine structure is likely to be limited by creep. This section assesses the structures and materials issues in the design of high temperature Si–SiC hybrid structures that have not been taken into consideration in the structural analysis to date.

First, it is unclear whether the structural design based on the values for the yield strength of Si used in the analysis is a conservative one. Fig. 10 shows stress-strain curves for Si at various levels of initial dislocation density. Measurements of the upper yield strength of Si [23], [24] have also shown that the upper yield strength of Si is a function of temperature, strain rate, and initial density of dislocations. The key question is whether or not the structural design of Si–SiC hybrid structures can rely on the upper yield strength of Si, which has been adopted for the allowable stress in the analysis so far. Some of the microfabrication processes such as the CVD process and thermal cycling may induce an increase of dislocation density within the Si crystal, which in turn may reduce the usable upper yield strength. Second, it is desirable that the service life of the Si–SiC hybrid turbine rotor be reliably estimated. At the temperatures of interest, the Si–SiC hybrid turbine rotor is susceptible to radial growth and blade distortion due to the creep of Si, effects which have not been accounted for in the previous FE analysis. While Walters performed a preliminary study of the Si creep and observed the localized deformation (an unexpected failure mechanism of single crystal Si consisting of slip bands), the creep parameters do not seem to be sufficiently accurate for design purpose [7], [8]. Finally, sharp corners such as blade roots or hub

Authorized licensed use limited to: UNIVERSITY OF SOUTHAMPTON. Downloaded on July 1, 2009 at 12:12 from IEEE Xplore. Restrictions apply.

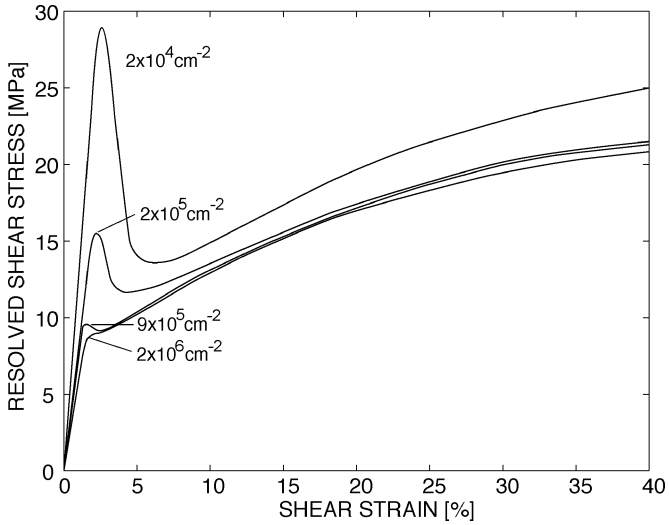

Fig. 10. Stress-strain curves of high-purity FZ-Si crystals in tensile deformation along the [123] direction as dependent on the initial density of dislocations. [K. Sumino, Deformation behavior of silicon, *Metallurgical and Materials Transactions A*, vol. 30A, pp1465–1479, 1999].

root, sites of high stress concentration, may be susceptible to structural instabilities when combined with the creep and strain softening of Si.

In order to design a structure safe from these concerns, it is imperative to develop a better material model for single crystal Si based on more rigorous mechanical testing at high temperatures. The model developed for this purpose is described elsewhere [23]–[25]. It consists of a continuum description of the plasticity of silicon, with nominal dislocation density and shear resistance as the internal variables. The model was calibrated on uniaxial compression creep tests, and subsequently validated on four point bend data for monolithic Si and Si–SiC beams. A good agreement between predictions and experimental data was achieved. In addition to the advanced Si material model, it is also crucial to assess the structural integrity of the Si–SiC hybrid structures including the interface between the Si and CVD SiC films (both the deposition and bonding interfaces) under the stresses and temperatures expected in service.

IV. Characterization of Mechanical Behavior of Si–SiC Hybrid Structures

This section discusses the mechanical testing results of Si–SiC hybrid structures and assesses the feasibility of the hybrid structures concept for elevated temperature micro-turbomachinery.

A. Mechanical Testing

Four-point bend testing with Si–SiC hybrid specimens as shown in Fig. 11 was chosen as a simple means to characterize the mechanical behavior of Hyper-Therm CVD SiC films at elevated temperatures and to prove the concept of Si–SiC hybrid microturbine structures. In terms of loading similarity, the CVD SiC films on the outer faces of the Si–SiC flexural specimens act as the reinforcement in a similar way to that expected in the Si–SiC hybrid microturbine rotor under centrifugal loading. Sandwich-type specimens with various SiC film thicknesses

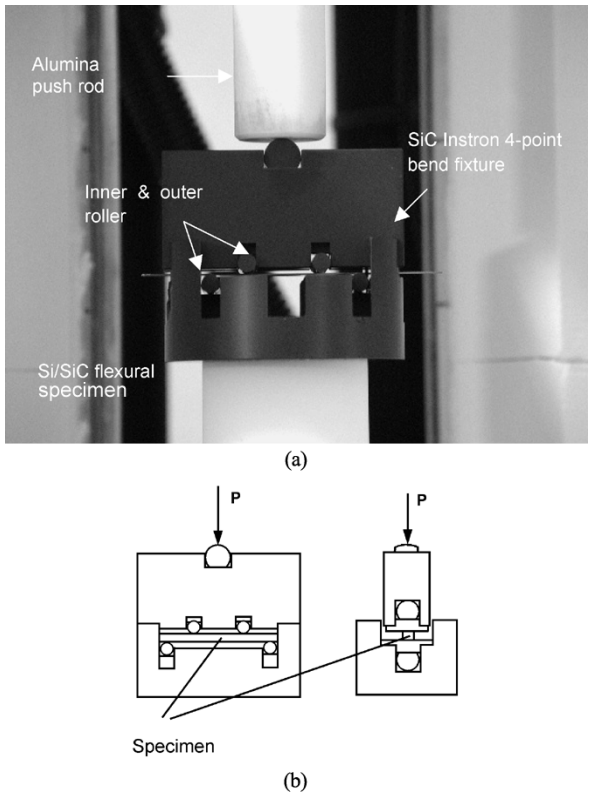

Fig. 11. (a) Four-point bend test setup and (b) schematic of the setup.

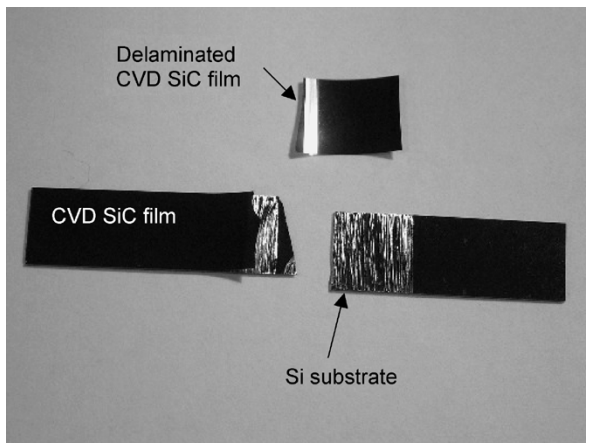

Fig. 12. Si–SiC bend specimen after testing at 850 °C and a ram speed of 0.001 mm/s.

were used in the four-point bend tests. Fig. 12 shows a Si–SiC flexural specimen after testing. The specimen dimensions are 0.5 mm thick, 8.8 mm wide, and 60 mm long. The specimen, coated with 15 μm thick CVD SiC films on both sides, was loaded until fracture at 850 °C and a ram speed of 0.001 mm/s. As shown in Fig. 12, the SiC film delaminated from the Si substrate on the tension side during the test. The SEM pictures in Fig. 13 clearly show the delaminated surface of the Si substrate with a high density of striations. The counterpart of the ridges on the Si substrate can be found on the delaminated SiC film. This implies that the fracture occurred in the Si and that the integrity of the Si–SiC interface was maintained during the plastic deformation at elevated temperatures.

Authorized licensed use limited to: UNIVERSITY OF SOUTHAMPTON. Downloaded on July 1, 2009 at 12:12 from IEEE Xplore. Restrictions apply.

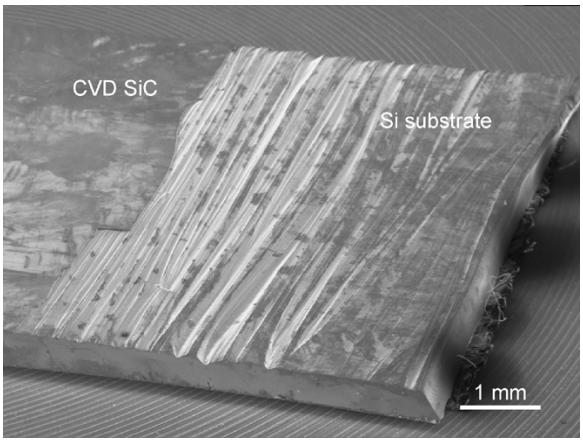

Fig. 13. SEM pictures of the Si–SiC flexural specimen with high density of striations left on the delaminated Si substrate after testing at 850 °C and a ram speed of 0.001 mm/s.

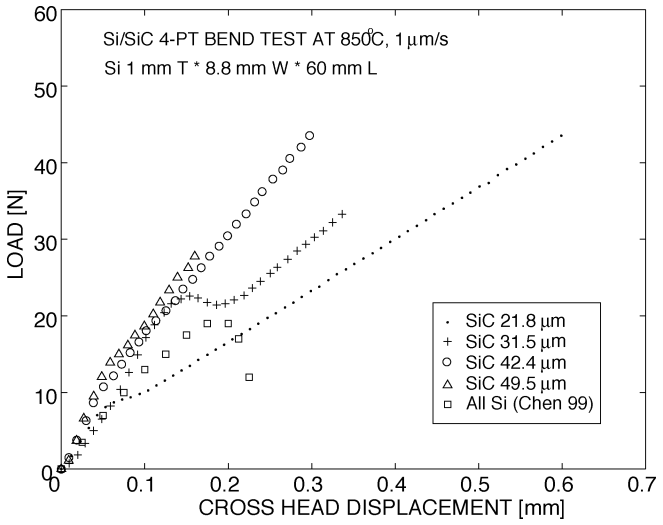

Fig. 14. Four-point bend test results of Si–SiC hybrid specimens with various SiC film thicknesses.

Four-point bend tests of the Si–SiC hybrid specimens were conducted for various SiC film thicknesses ranging from approximately 20 to 50 μm at 850 °C and 0.001 mm/s ram speed. The test results are plotted in Fig. 14. The all-silicon case is also plotted together for comparison. Each load-deflection curve changes its slope approximately at 10 N except for the case where the SiC film thickness is 31.5 μm. The initial slope can be obtained by the addition of the flexural rigidities of the Si substrate and SiC films. When the slope changes (or the Si substrate begins to yield), the maximum stress in the Si substrate is calculated to be approximately 20 MPa using composite beam theory, which is close to the flow stress of Si at 900 °C. From this point on, the thin CVD SiC films carry most of the load until fracture. Note that the slope after the Si yields increases with increasing the SiC film thickness.

Fig. 15 compares the model prediction of a Si–SiC 4-point bend test against the experimental data. The model accurately captures the temperature dependence originating from the plasticity of single crystal Si in combination with the elastic-brittle response of the SiC. The experimental data shows the relatively slow change in the initial nonlinear behavior compared to the

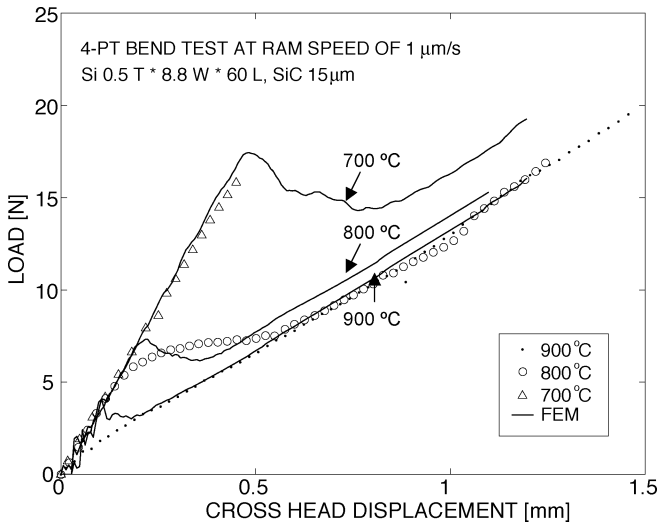

Fig. 15. Comparison of the model prediction against the four-point bend test results for Si–SiC hybrid specimens.

model prediction. It is speculated that the dislocations nucleated in the Si crystal during the CVD process or thermal cycling during the specimen preparation may reduce the peak load level, and then the shape of the nonlinear portion of the curves. In the analysis, no further assumptions were made to adjust the increased dislocation density in the Si crystal. The model prediction of a Si–SiC four-point bend test could be made more accurate by adopting a better assumption for the value of the dislocation density in the Si crystal.

From the experimental results and FE analysis results, it is clear that the thin CVD SiC films significantly increase the load-carrying capability of Si. While the usable load allowed by the all-silicon specimen is approximately 10 N (the plateau), the load that can be carried by the Si–SiC hybrid specimens is higher by approximately a factor of three. This considerable increase in the load-carrying capacity of Si–SiC hybrid specimens supports the overall concept of Si–SiC hybrid structures for elevated temperature micro-turbomachinery.

B. Fracture of Si–SiC Hybrid Structures

The fracture strength of CVD SiC films is also a key issue. The average stress in SiC films can be estimated by assuming an Si flow stress of 20 MPa. From bending moment equilibrium, the average stress in the SiC at fracture was found to range from 850 to 210 MPa, with the highest for the case of the 21.8 μm thick SiC film and the lowest for the case of the 49.5-μm-thick SiC film. Although the brittle nature of SiC films requires Weibull probabilistic analysis to characterize the fracture strength fully, it is believed that the thicker SiC films are intrinsically weaker due to differences in the process-induced defect population. It is worth noting that the fracture strength of CVD SiC is expected to be size dependent, which is favorable for the small scale devices such as the microengine. Also, process conditions and stress-states within the structures are the key factors determining the fracture strength of brittle materials.

Sudden load drops at the failure of the load-deflection curves in Fig. 14 may imply a brittle fracture of the Si–SiC specimens. Qualitatively, it appears that the Si substrate was subjected to

Authorized licensed use limited to: UNIVERSITY OF SOUTHAMPTON. Downloaded on July 1, 2009 at 12:12 from IEEE Xplore. Restrictions apply.

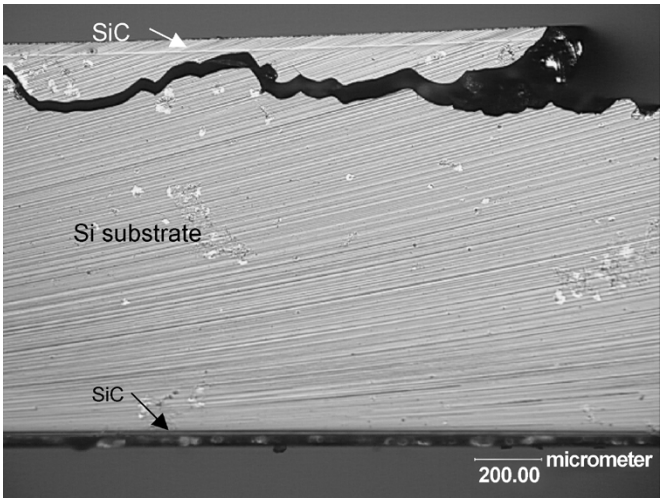

Fig. 16. Crack propagation in the Si substrate.

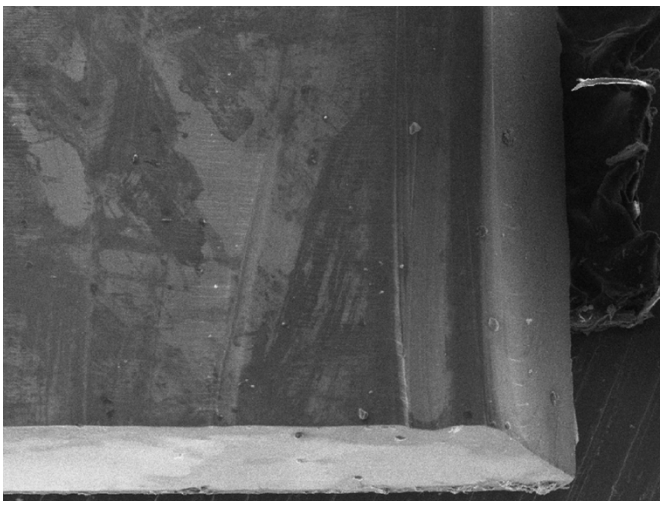

Fig. 17. SEM picture of a broken edge of the Si–SiC specimen loaded until fracture at 850 °C and a ram speed of 0.001 mm/s.

high strain rate loading due to the abrupt failure of the SiC film. The ductility of the Si substrate, however, does not seem to be sufficient to arrest cracks propagating from the SiC film or to sustain the fracture in a stable way. The Si–SiC specimens were also examined under an optical microscope at approximately 100x or similar at several intermediate deflections to locate any cracks that might have developed on the SiC films during the experiment, but no cracks were visible. Fig. 16 shows the crack propagation in the Si substrate underneath the SiC film on the tensile side of a specimen. The shiny ridges on the Si substrate in Fig. 12 appear to be an artifact of the crack propagation. Considering that there are no indications of any precursor event before fracture, such as sudden changes of the load in the load-deflection curves, the cracks seemed to propagate rapidly at the incident of fracture. Fig. 17 also shows the broken edge of the specimen, whose clean surface implies a fracture by cleavage.

V. Redesign of Si–SiC Hybrid Micro-Turbomachinery

Based on the knowledge derived from the experimental observations of the mechanical behavior of Si and Si–SiC hybrid structures together with the advanced Si constitutive model [23], [24], this section further evaluates the design of Si–SiC hybrid structures for high temperature micro-turbomachinery.

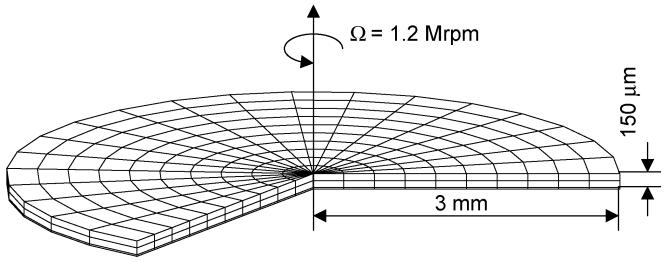

Fig. 18. Axisymmetric FE mesh to estimate the creep life of a Si–SiC hybrid turbine rotor.

A. Creep Life Estimation of a Si–SiC Hybrid Turbine Rotor

Miller [6] proposed a design based on a primitive material model for Si plasticity, consisting of a time independent elasto-perfectly plastic behavior. In this section, the design of a Si–SiC hybrid rotor is revisited with the Si model in order to provide a basis for reevaluating Miller's analysis.

1) FE Analysis Results for Creep Life Estimation of a Si–SiC Hybrid Turbine Rotor: An axisymmetric FE analysis was performed to estimate the creep life of the Si–SiC hybrid turbine rotor for various SiC relative thicknesses ranging from 0 to 30% at elevated temperatures. ABAQUS EXPLICIT was used together with the Si constitutive model implemented in a VUMAT user subroutine. A simple sandwich-type hybrid disc model with SiC reinforcement in between flat Si discs shown in Fig. 18 was used in the analysis, as was modeled by Miller [6]. The design specifications of the current microengine rotor were considered in this analysis. The SiC reinforcement was described as an elastic material with a Young's modulus of 430 GPa and Poisson's ratio of 0.21, as reported by Jackson for Hyper-Therm CVD SiC [26]. The FE model assumes a uniform temperature distribution on the hybrid disc and a rotational speed of 1.2 million rpm. It was assumed to take 10 s for the rotor to reach the design rotational speed to ensure a quasistatic analysis. The turbine rotor radial growth at the rim was calculated as a function of time using this axisymmetric FE model. The maximum tensile stress in the SiC reinforcement was also computed. This occurs at the rotational axis.

The FE simulation results for creep life estimation of a Si–SiC hybrid turbine rotor are shown in Fig. 19. The turbine rotor radial growth as a function of time is plotted for the four relative SiC thicknesses ranging from 0 to 30% for the temperatures, 700 and 900 °C. The radial growth for 10 seconds corresponds to the almost entirely elastic deformation of the turbine rotor while the rotor reaches the design rotational speed of 1.2 million rpm. As shown in Fig. 19, the all-silicon turbine rotor grows significantly more rapidly than the other cases with SiC reinforcement. Apparently, while the amount of SiC in the turbine rotor limits the overall turbine rotor radial growth by creep, the turbine wall temperature determines the time taken to reach a certain level of radial growth for a given thickness of CVD SiC in the turbine rotor. Thus, given the allowable turbine radial growth from the system considerations, the operating conditions

Authorized licensed use limited to: UNIVERSITY OF SOUTHAMPTON. Downloaded on July 1, 2009 at 12:12 from IEEE Xplore. Restrictions apply.

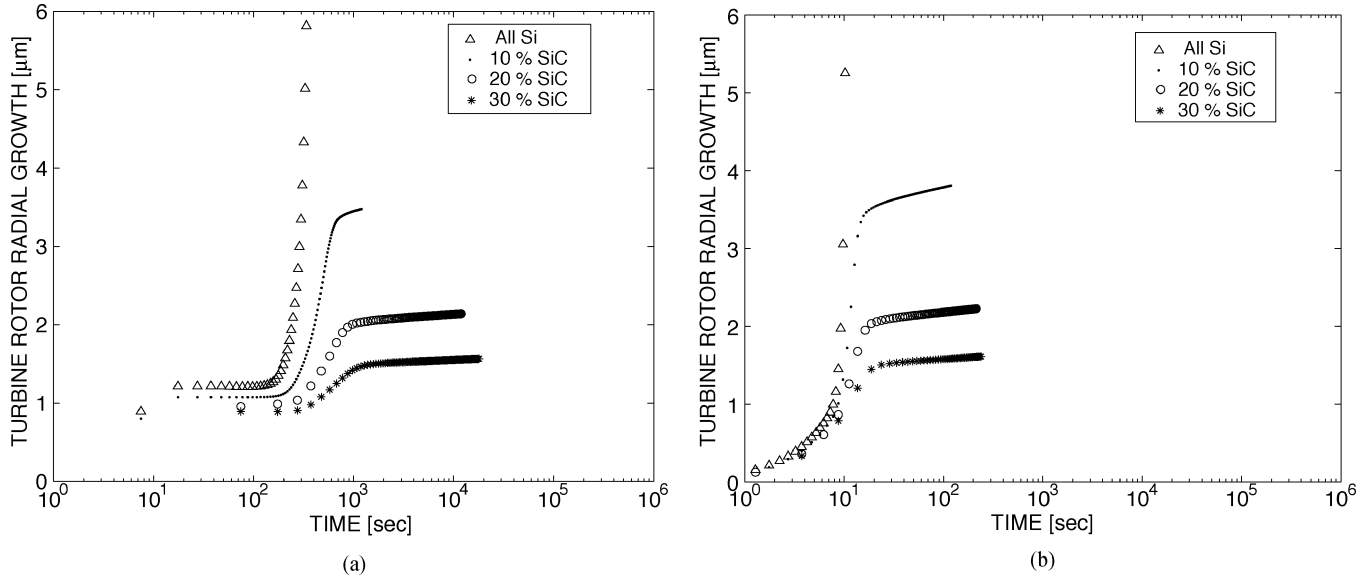

Fig. 19. Turbine rotor radial growth with time for various SiC relative thicknesses at various temperatures. (a) 700 °C; (b) 900 °C.

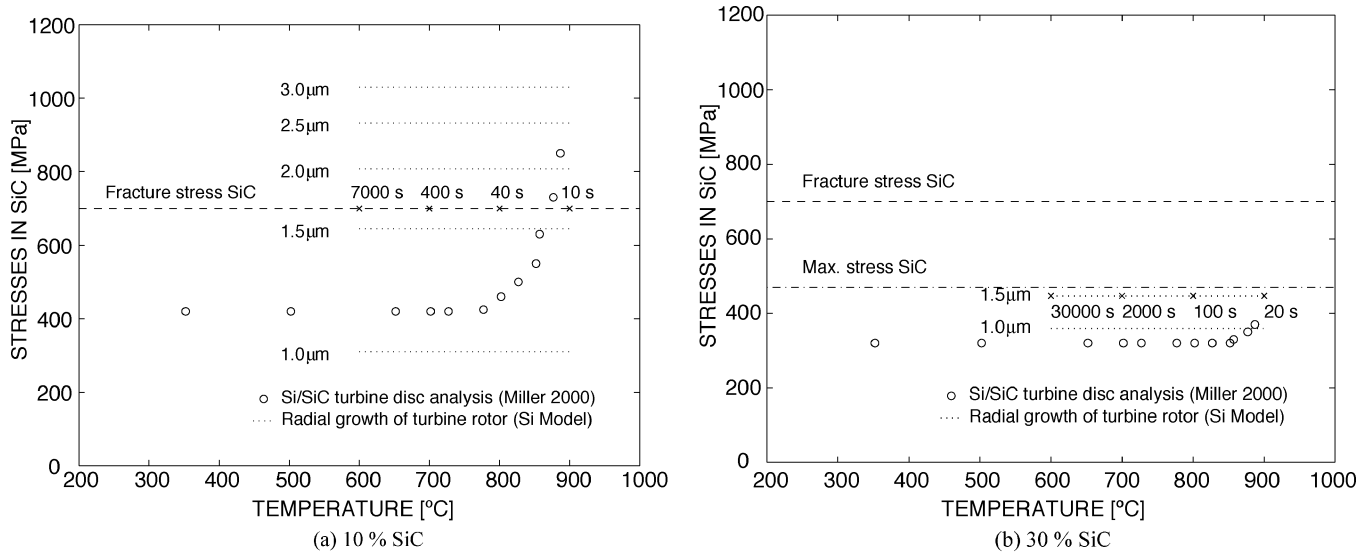

Fig. 20. Model prediction for creep life vs. elasto-plastic analysis (a) relative SiC thickness of 10% and (b) relative SiC thickness of 30%.

and minimum design requirements for Si–SiC hybrid structures can be extracted using these diagrams. In addition to failure due to creep of the Si, fracture of the SiC must be considered. At the microscale the dislocations nucleated within the Si crystal under the static load (centrifugal load) soften the Si structure, and consequently cause macroscale radial creep growth. As the Si creep proceeds, the load carried by the SiC reinforcement gradually increases. At a certain level of the turbine rotor radial growth, the stress in the SiC may reach its fracture strength. This is dependent on the relative thickness of SiC. This will be discussed in more detail in the next section.

2) Comparison of the Model Prediction for Creep Life and Elasto-Plastic Analysis: In Fig. 20, the maximum stress in the SiC is plotted against the turbine wall temperature. These results can be compared directly with those of Miller [6]. The elasto-plastic analysis shows the exponential growth of the stress in the SiC reinforcement with increasing temperature, but the data points are static at a given temperature. On the other hand, the stress in the SiC varies with time according to the model prediction at a given temperature, as the turbine radially grows with time. For the relative SiC thickness of 10%, the stress in the SiC reaches its assumed fracture strength of 700 MPa at the turbine radial growth of around 1.7 μm. According to the experimental results in the previous section, the SiC fracture strength of 700 MPa is easily achievable. However, this nominal strength represents a reasonably conservative value for design purposes. At 600 °C it takes approximately 2 h for the stress in the SiC reinforcement to reach the nominal fracture strength, and only 10 seconds at 900 °C. However, for the relative SiC thickness of 30%, the stress in the SiC reinforcement never reaches its fracture stress.

The elasto-plastic analysis by Miller [6] has also predicted a burst-line (temperature) for the hybrid turbine disc, beyond which the Si deforms severely and eventually bursts (numeri-

Authorized licensed use limited to: UNIVERSITY OF SOUTHAMPTON. Downloaded on July 1, 2009 at 12:12 from IEEE Xplore. Restrictions apply.

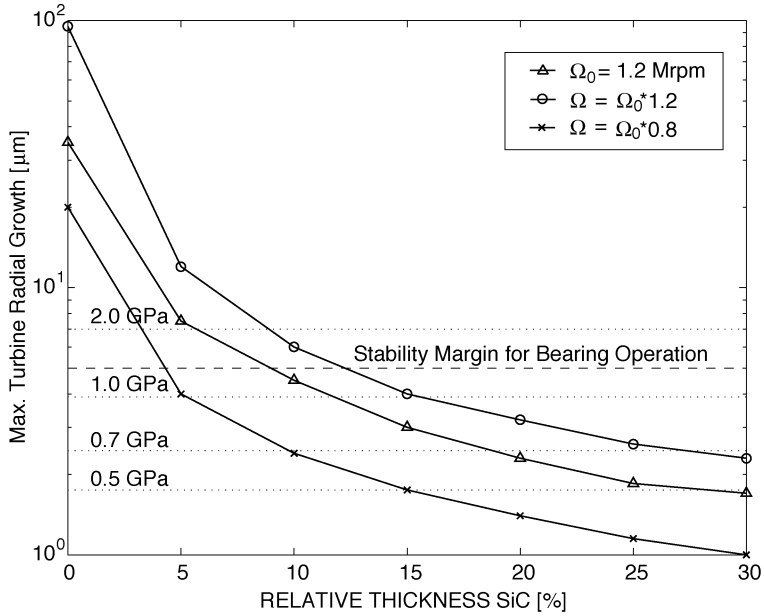

1. Rotational speed of the turbine rotor of 1.2 million rpm was used for a baseline in the analysis.
2. 10^6 seconds was used as a reference time for the maximum turbine radial growth.
3. Based on the analysis over the temperature range of 600 to 900 °C.
4. Stability margin for the bearing operation from Teo [27].

Fig. 21. Effect of SiC reinforcements on the radial growth of a Si–SiC hybrid turbine rotor.

cally the FEM, ABAQUS STANDARD, does not converge to a solution because of severe deformation of the Si). According to the results in Fig. 20(b), the structural integrity of the Si–SiC hybrid turbine, however, is not limited by the SiC fracture strength nor by the severe deformation of the Si. Instead, the structural integrity of the hybrid turbine rotor is likely to be limited by a time scale associated with overall system considerations. For example, the turbine rotor with a SiC layer of 10% relative thickness lasts for only 10 s at 900 °C. This rotor is obviously useless. However, depending on the allowable operating time for a device, the turbine rotor with a SiC layer of 10% relative thickness operating at 600 °C, which will eventually fail by fracture after 3 to 4 h, may be quite acceptable from a design point of view.

B. Design Criterion for the SiC Reinforcement of a Si–SiC Hybrid Turbine Rotor

Integrating all the information from the FE results presented in Section V-A, a criterion for the SiC reinforcement of a Si–SiC hybrid turbine rotor with regard to creep life is suggested in Fig. 21. The maximum turbine radial growth for the relative thickness of SiC was obtained from Fig. 20. Note that the relative SiC thickness determines the radial growth by creep almost irrespective of the turbine wall temperature. Here, 10^6 seconds was used as a reference time for the turbine service life, and the data are based on the analysis over the temperature range of 600 to 900 °C. Of course, depending on the reference time for the desired turbine operation, the whole curve can be adjusted, but not significantly. The dotted horizontal lines correspond to the various levels of the SiC fracture strength which given the relative thickness of SiC, correspond to the maximum stress in the SiC reinforcement at the reference time. From system considerations, such as the requirement for stable bearing operation, another horizontal line, corresponding to an allowable radial growth, can also be drawn as an additional constraint.

In order to illustrate the usage of the plot (i.e., Fig. 21), the following case was considered. Assuming the SiC fracture strength of 700 MPa and the stability margin for the bearing operation of 5 μm, the turbine rotor needs a SiC reinforcement with at least a relative SiC thickness of 20%. This configuration corresponds to a SiC layer of 60 μm for the design specifications of the current microengine rotor. This has been demonstrated in deposition experiments [9], [10]. Note that this design requirement is relatively conservative because Fig. 21 provides the relative SiC thickness based on the desired turbine service life of 10^6 seconds irrespective of the turbine wall temperature. The effect of the turbine rotor rotational speed was also considered. The reduction of the rotational speed by 20% allows for a thinner SiC layer down to the relative SiC thickness of 10%. This result implies that the level of the SiC reinforcement needs to be determined from the tradeoff between the overall system requirements and the constraints imposed by the microfabrication of Si–SiC hybrid structures. Moreover, it is clear that this design requirement on the SiC thickness is driven by the fracture strength of SiC for this case.

VI. Conclusion

The design space for the structural design of the microengine turbine rotor can be extended by incorporating SiC in the Si structures. The experimental results assessed the integrity of the Si–SiC interface during deformations at high temperatures as well as the material properties of CVD SiC. The significant increase in the load carrying capability of the Si–SiC hybrid specimens compared to the all-silicon specimens provides more de-

Authorized licensed use limited to: UNIVERSITY OF SOUTHAMPTON. Downloaded on July 1, 2009 at 12:12 from IEEE Xplore. Restrictions apply.

sign space for the design of the Si–SiC hybrid turbine rotor for the next generation microengine.

The use of a simple temperature-dependent, elastic-perfectly plastic constitutive law in the initial stages of design was useful as it allowed for the relatively rapid comparison of design options. However, in validating the overall design and to perform life prediction, it is necessary to use a more sophisticated model that is capable of properly accounting for rate effects.

ACKNOWLEDGMENT

The authors would like to acknowledge A. Mracek for her assistance in conducting the experiments. The cooperation of the staff of the Microsystems Technology Laboratories (MTL), the Technology Laboratory for Advanced Composites (TELAC), and the Center for Material Sciences (CMSE) at MIT are also acknowledged.

REFERENCES

[1] H. Epstein *et al.*, "Power MEMS and microengines," in *Proc. IEEE Conference on Solid State Sensors and Actuators*, 1997.
[2] K. A. Lohner, "Microfabricated Refractory Ceramic Structures for Micro Turbomachinery," S. M. thesis, Dept. of Aeronautics and Astronautics, MIT, Cambridge, MA, 1999.
[3] J. Protz, "The Design and Development of a MEMS Silicon Micro Gas Turbine Engine," Ph.D. dissertation, Dept. of Aeronautics and Astronautics, MIT, 2000.
[4] A. Ayon, D. Choi, T. Harrison, E. Huang, B. Miller, H.-S. Moon, E. Noonan, S. M. Spearing, K. Turner, and X. Zhang, "Materials, Structures, and Packaging Annual Technical Report, The MIT Micro-engine Project,", Dec. 1999.
[5] K. A. Lohner, K.-S. Chen, A. A. Ayon, and S. M. Spearing, "Microfabricated silicon carbide microengine structures," in *Mater. Res. Soc. Symp. Proc.*, vol. 546, 1999, pp. 85–90.
[6] B. Miller, "Hybrid Silicon/Silicon Carbide Microstructures and Silicon Bond Strength Tests for the MIT Microengine," S. M. thesis, Dept. of Aeronautics and Astronautics, MIT, Cambridge, MA, 2000.
[7] D. S. Walters, "Creep Characterization of Single Crystal Silicon in Support of the MIT Micro-Engine Project," M.S. thesis, Dept. of Mechanical Engineering, MIT, Cambridge, MA, 1999.
[8] D. S. Walters and S. M. Spearing, "On the flexural creep of single crystal silicon," *Scripta Materialia*, vol. 42, pp. 769–774, 2000.
[9] K. A. Lohner, "Microfabricated Refractory Ceramic Structures for Micro Turbomachinery," S. M. Thesis, Dept. of Aeronautics and Astronautics, MIT, Cambridge, MA, 1999.
[10] M. Mehregany, C. A. Zorman, N. Raja, and C. H. Wu, "Silicon carbide MEMS for harsh environments," *Proc. IEEE*, vol. 86, pp. 1594–1610, Aug. 1998.
[11] D. Choi, R. J. Shinavski, and S. M. Spearing, "Process development of silicon-silicon carbide hybrid micro-engine structures," in *Mater. Res. Soc. Symp. Proc.*, vol. 687, Fall 2001, p. B5.44.
[12] R. J. Shinavski and W. S. Steffier, "Enhanced Strength, Nanolayered SiC for Micro Gas Turbine Portable Power Generation," Hyper-Therm Inc., 1999.
[13] J. A. Powell, L. G. Matus, and M. A. Kuczmarski, "Growth and characterization of cubic SiC single-crystal films on Si," *J. Electrochem. Soc.*, vol. 134, pp. 1558–1565, 1987.
[14] A. J. Fleischman, C. A. Zorman, M. Mehregany, C. Jacob, S. Nishino, and P. Pirouz, "Epitaxial growth of 3C-SiC films on 4-inch diameter (100) silicon wafers by APCVD," in *Proc. of the Sixth International Conference, Silicon Carbide and Related Materials 1995*, 1996, pp. 197–200.
[15] C.-H. Wu, C. A. Zorman, and M. Mehregany, "Characterization of polycrystalline SiC grown on SiO_2 and Si3N4 by APCVD for MEMS applications," *Mater. Sci. Forum*, pt. 1, vol. 338–342, pp. 541–544, 2000.
[16] C. C. Chiu, S. B. Desu, and C. Y. Tsai, "Low pressure chemical vapor deposition (LPCVD) of β-SiC on Si (100) using MTS in a hot wall reactor," *J. Mater. Res.*, vol. 8, no. 10, pp. 2617–2626, 1993.
[17] D. Choi, "Characterization of CVD SiC for Microengine Applications: Residual Stress Control and Microfabrication," Ph.D. dissertation, Dept. of Materials Science and Engineering, MIT, Cambridge, MA, 2003.
[18] M. A. Schmidt, "Wafer-to-wafer bonding for microstructure formation," *Proc. IEEE*, vol. 86, p. 1575, Aug. 1998.
[19] *MSC/PATRAN Reference Manuals*, 2001.
[20] *ABAQUS Reference Manuals*, Providence, RI, 2001.
[21] K.-S. Chen, "Materials Characterization and Structural Design of Ceramic Micro Turbomachinery," Ph.D. dissertation, Dept. of Mechanical Engineering, MIT, Cambridge, MA, 1999.
[22] B. Philippon, S. M. Thesis, Dept. of Aeronautics and Astronautics, MIT, Cambridge, MA, 2001.
[23] H.-S. Moon, S. M. Spearing, and L. Anand, "A constitutive model for single crystal Si at elevated temperature: I—model development," J. Eng. Mater. Technol., 2003, submitted for publication.
[24] ——, "A constitutive model for single crystal Si at elevated temperature: II—applications," J. Eng. Mater. Technol., 2003, submitted for publication.
[25] H.-S. Moon, "Design of Si/SiC Hybrid Structures for Elevated Temperature Micro-Turbomachinery," Ph.D. dissertation, MIT, Cambridge, MA, 2002.
[26] K. Jackson, R. Edwards, and W. Sharpe Jr., "Mechanical properties of thin film silicon carbide," in *Mat. Res. Soc. Symp. Proc.*, vol. 687, Fall 2001, p. B6.3.
[27] C. J. Teo, "Personal Communications," unpublished, 2002.

Hyung-Soo Moon received the B.S. and M.S. degrees in mechanical engineering from Seoul National University, Seoul, Korea, in 1992 and 1995, respectively, and the Ph.D. degree in mechanical engineering from the Massachusetts Institute of Technology (MIT), Cambridge, in 2002 with a dissertation on the design of Si–SiC hybrid structures for elevated temperature micro turbomachinery.

He is currently a Postdoctoral Associate at MIT, mainly responsible for the materials and structures issues associated with the development of the next generation MIT Microengine. His recent research activities also include the numerical modeling of gold thermocompression wafer bonding and the development of a novel photomask for optical lithography consisting of dense arrays of nanowires/nanotubes using the self-assembly of diblock copolymer.

Dongwon Choi is currently a graduate research assistant pursuing the Ph.D. degree in the Department of Materials Science and Engineering at the Massachusetts Institute of Technology (MIT), Cambridge.

Since 1999, he has been with the Gas Turbine Laboratory at MIT, where he is working on silicon carbide process development for power-MEMS applications. His research interests include advanced microfabrication technologies, micro- and nanoscale materials and structures in MEMS devices, in particular, mechanical properties, residual stresses and related issues in deposited materials.

S. Mark Spearing received the Ph.D degree from Cambridge University Engineering Department in 1990.

He is a Professor of Aeronautics and Astronautics at the Massachusetts Institute of Technology (MIT), Cambridge, where he has been since 1994. In 2004, he became a Professor of Engineering Materials at the University of Southampton, U.K. His technical interests include materials characterization and structural analysis and design of MEMS, development of wafer bonding-technologies, microelectronic and MEMS packaging and advanced composites. Since 1995 he has been responsible for materials, structural design and packaging tasks of the MIT MicroEngine, MicroRocket, Micro-Chemical Power and MicroHydraulic Transducer projects as well as conducting cross-cutting underpinning technology development. He is an editor of the JOURNAL OF MICROELECTROMECHANICAL SYSTEMS.

Dr. Spearing is a Member of the American Society of Mechanical Engineers (ASME).

Authorized licensed use limited to: UNIVERSITY OF SOUTHAMPTON. Downloaded on July 1, 2009 at 12:12 from IEEE Xplore. Restrictions apply.